universe

MDPI

Article

Quantized Nuclear Recoil in the Search for Sterile Neutrinos in Tritium Beta Decay with PTOLEMY

Wonyong Chung, Mark Farino, Andi Tan, Christopher G. Tully * and Shiran Zhang

Department of Physics, Princeton University, Princeton, NJ 08544, USA; wonyongc@princeton.edu (W.C.); mfarino@princeton.edu (M.F.); andit@princeton.edu (A.T.); srzhang@princeton.edu (S.Z.)
* Correspondence: cgtully@princeton.edu

Abstract

The search for keV-scale sterile neutrinos in tritium beta decay is made possible through the theoretically allowed small admixture of electron flavor in right-handed, singlet, massive neutrino states. A distinctive feature of keV-scale sterile-neutrino–induced threshold distortions in the tritium beta spectrum is the presence of quantized nuclear-recoil effects, as predicted for atomic tritium bound to two-dimension materials such as graphene. The sensitivities to the sterile neutrino mass and electron-flavor mixing are considered in the context of the PTOLEMY detector simulation with tritiated graphene substrates. The ability to scan the entire tritium energy spectrum with a narrow energy window, low backgrounds, and high-resolution differential energy measurements provides the opportunity to pinpoint the quantized nuclear-recoil effects. providing an additional tool for identifying the kinematics of the production of sterile neutrinos. Background suppression is achieved by transversely accelerating electrons into a high magnetic field, where semi-relativistic electron tagging can be performed with cyclotron resonance emission RF antennas followed by deceleration through the PTOLEMY filter into a high-resolution differential energy detector operating in a zero-magnetic-field region. The PTOLEMY-based approach to keV-scale searches for sterile neutrinos involves a novel precision apparatus utilizing two-dimensional materials to yield high-resolution, sub-eV mass determination for electron-flavor mixing fractions of $|U_{e4}|^2 \simeq 10^{-5}$ and smaller.

Keywords: PTOLEMY; keV; sterile; neutrino; tritium; beta decay; graphene; semi-sudden approximation; warm dark matter

check for updates

Academic Editors: Lorenzo Iorio and Norma G. Sanchez

Received: 15 July 2025
Revised: 19 August 2025
Accepted: 26 August 2025
Published: 2 September 2025

Citation: Chung, W.; Farino, M.; Tan, A.; Tully, C.G.; Zhang, S. Quantized Nuclear Recoil in the Search for Sterile Neutrinos in Tritium Beta Decay with PTOLEMY. *Universe* **2025**, *11*, 297. https://doi.org/10.3390/universe11090297

Correction Statement: This article has been republished with a minor change. The change does not affect the scientific content of the article and further details are available within the backmatter of the website version of this article.

Copyright: © 2025 by the authors. Licensee MDPI, Basel, Switzerland. This article is an open access article distributed under the terms and conditions of the Creative Commons Attribution (CC BY) license (https://creativecommons.org/licenses/by/4.0/).

1. Introduction

The existence of right-handed neutrinos follows from the discovery of finite neutrino masses through oscillation experiments. Within the Standard Model of Particle Physics, the right-handed neutrinos have no gauge interactions and are therefore dubbed "sterile." With active left-handed and sterile right-handed components, the neutrinos will have Dirac mass terms. The right-handed components can form Majorana mass terms due to their sterility [1]. Chirality suppression does not apply to right-handed mass terms, and therefore the range of masses in the sterile neutrino sector can be expansive, with substantial mixing of lepton flavors across mass eigenstates, as observed in the PMNS neutrino matrix [2–6]. It is in this unique context that one looks into the dark, weakly coupled sector of neutrinos to find answers to outstanding questions on the structure and evolution of the universe. Among these are the components of dark matter: yet-to-be-discovered, primarily gravitationally interacting forms of matter that, through the Hubble

expansion history of the universe, are consistent with particles that are nonrelativistic in the present day. The search for keV-scale sterile neutrinos is strongly motivated by the observational data from galaxies at distances below 100 kpc that could be explained if a substantial fraction of dark matter consisted of keV-scale particles as opposed to solely consisting of particles with masses at the GeV scale or higher [7].

Warm dark-matter studies that test for a keV-scale sterile-neutrino fraction encompass a range of potential observables, including rates of decay of heavy neutrinos into an X-ray and a light neutrino [8,9]. Searches for anomalous X-rays from keV-scale decay of sterile neutrinos place limits on the set of model parameters that determine sterile–active neutrino mixing, the fraction of dark-matter energy density contributed by sterile neutrinos and sterile neutrino masses [10]. However, there are nonstandard models for keV-scale sterile-neutrino dark matter that remain consistent with the bounds set by observational data and may explain the rapid early formation of supermassive black holes that seeded early galaxy formation [11–13]. Several other aspects of warm dark-matter physics are strongly constrained by early-universe production, freeze out, prerecombination and 21 cm line observables [14,15].

In this study, we look at a new approach to identifying keV-scale production of sterile neutrinos in the β-decay of tritium. The threshold production physics of massive neutrinos has served as the primary tool for searches since the earliest studies of the β-decay spectrum distortions [16]. These predictions are for free nuclei. In the context of the PTOLEMY experiment with a tritiated-graphene substrate, the high resolution on the electron measurement is shown to make it possible to identify threshold physics unique to the graphene substrate. Through a series of spectrum fits, the sensitivity to energy-spectrum distortions near the sterile-neutrino production threshold, arising from quantized nuclear-recoil effects, is demonstrated. The current state of the art for searches for sterile neutrinos in the tritium beta decay spectrum is implemented by TRISTAN [17]. Related studies on the KATRIN spectrometer of the TRISTAN experiment show potential sources of tritium-spectrum distortion that lead to potential limiting systematics and complexities in the high-precision analysis of the tritium spectrum for keV-scale sterile-neutrino features [18]. An additional observable in the threshold behavior of the production of sterile neutrinos, as proposed here, could potentially resolve systematic contributions that fake a sterile-neutrino threshold.

First, we review the configuration and capabilities of the PTOLEMY detector in the context of a search for sterile neutrinos. We then describe the models that characterize quantized nuclear recoil for tritiated graphene. In the subsequent section, the simulation results on the sensitivities for mixing angle and neutrino mass are presented for a range of mixing angles. Finally, a discussion follows on how quantized nuclear-recoil effects from tritiated graphene are a tell-tale signature that confirms the expected threshold physics of the production of sterile neutrinos.

2. PTOLEMY for a Search for Sterile Neutrinos

A program to search for sterile neutrinos as part of the PTOLEMY experimental work has been considered previously [19,20]. In light of recent developments regarding theoretical predictions for the β-decay spectrum of tritiated graphene, the search for sterile neutrinos is revisited, considering the possibility of a new observable in the threshold behavior [21].

The PTOLEMY spectrometer can be operated with a narrow energy window to analyze electrons that are produced near the maximum kinematic energy corresponding to the production threshold of a given sterile-neutrino candidate over the 18.6 keV range of the tritium beta decay kinematics. The PTOLEMY spectrometer can set a lower and an

upper limit for the energy window. Therefore, electron measurements can be taken over a dedicated region of the spectrum. For electrons in this energy window, a transverse-drift acceleration process increases the kinetic energy of the electrons and transports them into the high-magnetic-field region of the radio-frequency (RF) cyclotron emission-tagging system. In this region, the electrons travel semirelativistically transverse to the magnetic field and radiate an RF signal within the roughly 10 μs time interval of the tagging region. The RF tag strongly suppresses nonelectron backgrounds in time coincidence with the microcalorimeter or electrostatic spectrometer differential energy measurement at sub-eV energy resolution [22,23]. A simulation render of the PTOLEMY setup is shown in Figure 1. A narrow filter-energy window, on the order of 200 eV wide, will suppress the total calorimeter rate by two orders of magnitude or more by restricting the measurement to selected ranges of sterile neutrino mass. This is a strategy that can be used to enhance sensitivity to threshold detection for low-mixing-angle searches that are statistically limited, especially when the mass of the candidate sterile neutrino is guided by accelerator or astrophysical signatures. The high resolution of the differential energy measurements of the PTOLEMY approach will directly record the footprint of the low-momentum recoil behavior of ^{3}He from the quantized effects of its interactions with the graphene substrate at the kinematic endpoint [21]. Direct measurement of quantized neutrino-recoil effects in the searches for light neutrinos at the endpoint will provide a clear prediction for keV-scale production of sterile neutrinos in the region of the threshold.

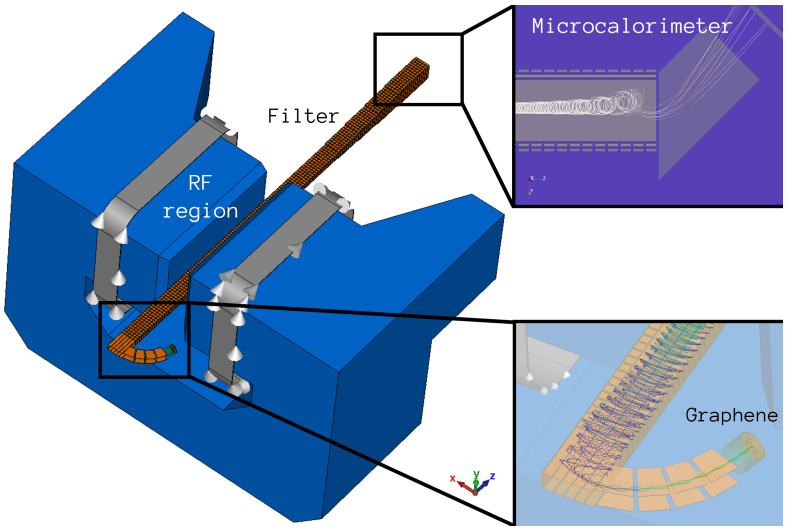


Figure 1. A simulation render of the PTOLEMY demonstrator apparatus used in searches for sterile neutrinos, showing the iron yoke (blue), coils (gray), and electrodes (orange). (bottom right) Electrons from a tritiated-graphene source (round disk) in the fringe field region of the magnet are collimated and transported into the central field region using a modular approach to increase instrumented mass. Sample trajectories of 18.6 keV endpoint electrons with pitch angles in the range 5–85 degrees are shown. Once they are in the center region, the electrons are accelerated into the uniform 1 T field region between the iron pole faces for CRES RF tagging. (top right) After they have been transported through the RF and transverse-drift filter, electrons exit the filter and enter an electrostatic lensing configuration; this leads to an electrostatic spectrometer or a TES microcalorimeter housing, which is not shown in the main image.

3. Quantized Nuclear Recoil

Three models describing the range of theoretical predictions for the tritiated graphene β-decay-spectrum endpoint have been proposed [21]. In this study, a set of parameter choices is used to describe the models. Direct measurements at the endpoint, as planned by the PTOLEMY collaboration, are needed to fix these parameters to a given production of

tritiated-graphene samples. The three models are described as the sudden, semi-sudden, and adiabatic approximations, with each yielding different quantized nuclear-recoil (QNR) effects on the β spectrum. In the sudden and semi-sudden approximations, the resultant spectrum receives contributions both when the daughter ^{3}He is freed from the graphene and when it remains bound. In the case of adiabatic approximations, there are no bound states, and hence there is a contribution only when ^{3}He is freed.

QNR effects make it possible to distinguish a sterile-neutrino signal from anomalous bumps present in the recorded tritium β spectrum (such as an undetected X-ray emission within the substrate). Explicitly, the sterile-neutrino threshold would replicate QNR effects present at the β spectrum endpoint; in the case of the semi-sudden or sudden approximation, this would manifest in spectrum contributions both when the daughter ^{3}He is freed and when it remains bound, resulting in an additional bump due to slightly differing endpoints. One would thus be able to properly identify a sterile-neutrino signal in these instances by demonstrating superior fitting capability using a sudden/semi-sudden model compared to a single bump 'null hypothesis' (i.e., an adiabatic fitting model).

4. Simulation Results

In this study, we look to characterize the PTOLEMY demonstrator's sensitivity to sterile-neutrino detection based on an expected exposure of 300 μg · years, with primary emphasis on the impact of PTOLEMY's high-resolution transition-edge sensor microcalorimeter [24]. Thus, we compare results between $\sigma = 50$ meV and $\sigma = 50$ eV with equal exposure to highlight the benefit of high-resolution energy measurements. For simplicity, we assume $\sim 100\%$ detector efficiency, equating an exposure of 300 μg · years to 10^{18} recorded events. However, these results can identically be viewed as exposure over a longer time window or with a larger target at some nonunity efficiency (i.e., 300 μg · years at 100% efficiency yields identical event totals to 600 μg · years at 50% efficiency).

We model the resulting β spectrum of neutrino production from a tritiated-graphene substrate as an equally-weighted combination of two Fermi β decay spectra. With slightly differing endpoint energies, the two components serve as an approximation to spectrum contributions when the daughter ^{3}He either remains bound or becomes freed from the graphene. Two sets of these spectra are generated: one in which m_ν is fixed at 200 meV (i.e., a plausible electron neutrino mass m_β) and one with $m_\nu \in [1\text{ keV}, 18\text{ keV}]$ (a keV-scale sterile neutrino with energy below the tritium endpoint). The contribution of the sterile neutrino is then weighted relative to the electron neutrino component according to a small mixing angle $\sin^2\theta$. The separation between bound and free endpoint energies depends on the chosen QNR approximation. To illustrate this point, the difference in endpoint energy between the free and bound ^{3}He contribution for the sudden (semi-sudden) approximation is 7 eV (49 eV) in this study. Again, no bound states are present in the adiabatic approximation. Future measurements by PTOLEMY of the quantized nuclear-recoil effects at the tritium endpoint and further theoretical study are essential to tack down the parameters that describe the threshold physics model for tritiated-graphene. Once these parameters are known at the endpoint, they can be applied directly to a sterile-neutrino search via spectrum fitting.

The combined electron and sterile neutrino spectrum is convolved with a Gaussian to account for energy resolution. Simulated data are generated by finely binning this underlying distribution, scaling to a desired level of exposure, and finally fluctuating each bin according to Gaussian counting statistics. Assuming an exposure of 300 μg · years for the PTOLEMY demonstrator, $\sim 10^{18}$ events are expected for the total β-spectrum, though we only examine a small 200 eV energy window centered around sterile neutrino threshold effects. In such a window, we observe only a fraction of this event total (e.g., a 200 eV

window centered around a threshold produced by a 7 keV sterile neutrino only contains ∼0.7% of the total electron neutrino spectrum, and an even smaller portion of the sterile neutrino spectrum).

Levels of fitted parameter error and model differentiation remain fairly consistent across the three approximations. To thus mitigate redundancy, we show results for only simulated data generated under the semi-sudden approximation. Figure 2 presents a 200 eV window of simulated data centered around the threshold effects of a 7 keV sterile neutrino with mixing angle $\sin^2\theta = 0.1$ (for visibility) for both energy resolution of 50 meV and 50 eV. Bound and free contributions to sterile-neutrino production are evident in high-resolution energy measurements, producing discernible kinks in relation to the m_β portion of the spectrum; however, these kinks vanish at a coarser resolution.

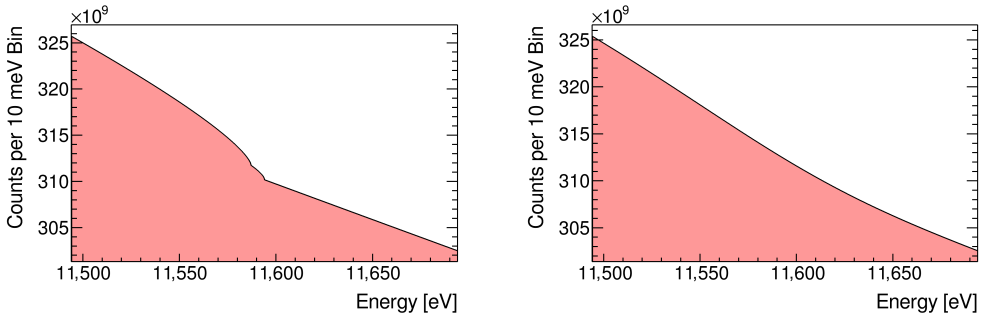


Figure 2. An example 200 eV window of binned β electron energy data generated from 300 µg · years of tritium β-decay exposure (100% efficiency) centered around the threshold of a 7 keV sterile neutrino with a mixing angle of $\sin^2\theta = 0.1$ according to the semi-sudden approximation. Data are smeared with (**a**) 50 meV and (**b**) 50 eV energy resolution via Gaussian convolution, and each 10 meV-wide bin is fluctuated according to Gaussian counting statistics. QNR effects from production of sterile neutrinos are visible in the case of higher energy resolution.

4.1. Parameter Extraction for Various $\sin^2\theta$ *and* m_ν

Using this data-simulation procedure, fits are performed in which both $\sin^2\theta$ and m_ν are floated (alongside the overall function scaling) to estimate the errors in extracting these quantities for a given input. Discretizing the ranges $m_\nu \in [1\,\text{keV}, 18\,\text{keV}]$ and $\sin^2\theta \in [10^{-8}, 10^{-4}]$ into 100 steps each (linearly and logarithmically spaced, respectively), 10,000 unique parameter settings are studied for both 50 meV and 50 eV resolutions. For each setting, 100 fits to unique Gaussian-fluctuated data sets are performed to obtain an average estimate on fitting power for each parameter. Figure 3 presents the mean absolute percent error between fitted and input mixing angle $\sin^2\theta$, where the value is capped at 100%. Percent error was chosen as an output to roughly gauge both bias and general fluctuation in fitting, whereas the use of sensitivity would require a separate bias study. We observe only minimal improvement at higher resolution, noting that an average fitted value within 30% of truth occurs around $\sin^2\theta \gtrapprox 10^{-6}$ and $m_\nu \gtrapprox 3$ keV for both. While we observe visible obfuscation of threshold effects associated with the production of sterile neutrinos in Figure 2 for a larger energy resolution, fitting power for $\sin^2\theta$ remains largely consistent, as it predominantly depends on the distribution of events within the 200 eV window (regardless of energy resolution, sterile and electron neutrino contributions to the β spectrum yield characteristically different relative event distributions near the sterile-neutrino threshold). A larger discrepancy would likely be seen if relative uncertainty on energy resolution were considered.

Shifting the focus to fitting output on sterile-neutrino mass, m_ν, we observe a significant deterioration of output accuracy correlated to coarsened energy resolution. Figure 4

presents the mean absolute difference on the fitted mass vs. truth (to again gauge average fitting bias and error) for energy resolutions of both 50 meV and 50 eV. As we fit only within the 200 eV window, the outputted mean absolute difference is necessarily capped at 100 eV. In the case of a 50 meV energy resolution, the average difference hardly ever exceeds 20 eV and is consistently below 10 eV for the majority of the phase space. A coarser resolution of 50 eV, however, leads to significantly worse fitting capability, with average differences approaching 80 meV for small mixing angles. Intuitively, the power of the fit to resolve threshold effects lessens as the nondifferentiable threshold kinks are smoothed by coarser resolution. This suggests m_ν is much more strongly correlated with resolution than mixing angle, indicating PTOLEMY will have the capability to perform an eV-level (if not sub-eV-level) measurement of m_ν of a sterile neutrino present in the spectrum window. This relational advantage would be further enhanced if one were to consider a relative uncertainty in the energy resolution.

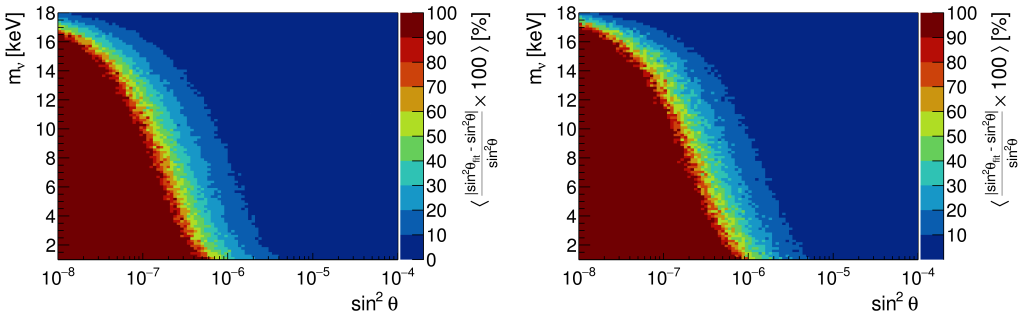


Figure 3. Mean absolute percent error between fitted and input $\sin^2\theta$ obtained in fit for $m_\nu \in [1\,\text{keV}, 18\,\text{keV}]$ and $\sin^2\theta \in [10^{-8}, 10^{-4}]$ using 300 μg · years of semi-sudden approximation tritium data smeared with (**a**) 50 meV and (**b**) 50 eV energy resolution. Each cell performs fits to 100 different Gaussian-fluctuated (200 eV window) data sets and tabulates the average percent difference between $\sin^2\theta$ obtained from the fit and the original input. The output percent difference is capped at 100%. Minimal improvement is seen as a result of high-resolution energy measurements, with an average fitted value within 30% of truth occurring around $\sin^2\theta \gtrapprox 10^{-6}$ and $m_\nu \gtrapprox 3$ keV for both.

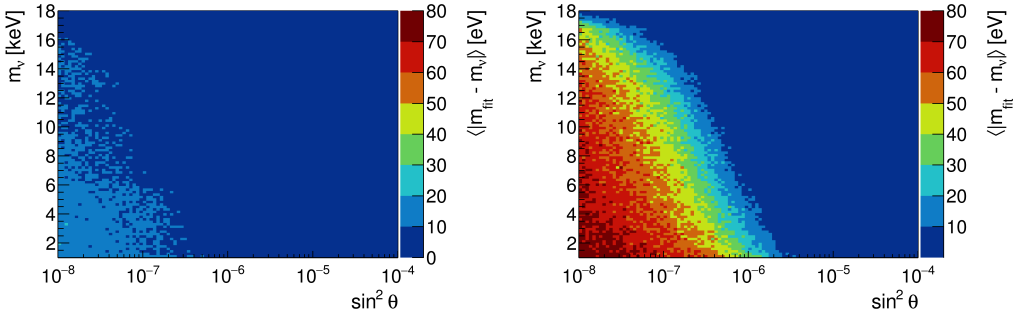


Figure 4. Mean absolute difference between fitted and input m_ν obtained in fit for $m_\nu \in [1\,\text{keV}, 18\,\text{keV}]$ and $\sin^2\theta \in [10^{-8}, 10^{-4}]$ using 300 μg · years of semi-sudden approximation tritium data smeared with (**a**) 50 meV and (**b**) 50 eV energy resolution. Each cell performs fits to 100 different Gaussian-fluctuated (200 eV window) data sets and tabulates the average absolute difference between m_ν obtained from the fit and the original input. Because the fit only occurs within the data window, the output is necessarily capped at 100 eV. Drastic improvement is seen as a result of high-resolution energy measurements, indicating a significantly higher sensitivity to an eV-level precision measurement of m_ν.

4.2. Separation Power of the QNR Model

In Figure 5, we perform fits using all three approximations to the semi-sudden simulated data previously shown in Figure 2, again with respective resolutions of 50 meV and 50 eV. With a large mixing angle of $\sin^2\theta = 0.1$ to visualize the effect, we observe characteristic differences in the three models dissipate as energy resolution coarsens.

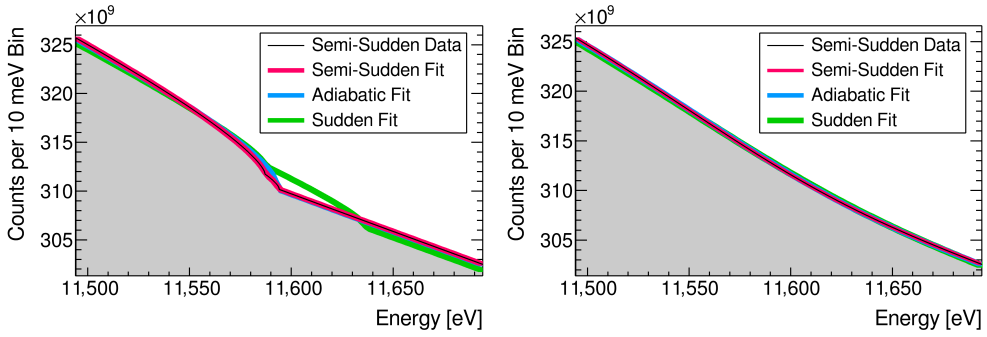


Figure 5. A 200 eV window of data generated from 300 μg · years of tritium exposure centered around the threshold of a 7 keV sterile neutrino with mixing angle $\sin^2\theta = 0.1$ according to the semi-sudden approximation. Fits with floating parameters m_ν and $\sin^2\theta$ (as well as overall amplitude as a nuisance parameter) are shown for functions derived under the adiabatic, sudden, and semi-sudden approximations. Data and fitting functions are smeared with (**a**) 50 meV and (**b**) 50 eV energy resolution. The three functions are visibly distinguishable in the case of high-resolution energy measurements, although the functions become mutually indistinguishable as resolution coarsens.

To quantify this effect and estimate PTOLEMY's sensitivity to model discrimination, we report the average goodness of fit (χ^2 per number of degrees of freedom [n. d. f.] as averaged over 100 fits) on semi-sudden data ($m_\nu = 7$ keV, $\sin^2\theta = 10^{-5}$) for models derived from each approximation and resolution combination as a function of total exposure in Figure 6. To clarify, 50 eV-smeared functions are fit only to 50 eV resolution data, and 50 meV-smeared functions are fit only to 50 meV resolution data. The parameters, m_ν and $\sin^2\theta$, and the overall function scaling are floating in each fit. In the case of semi-sudden models for both resolutions, χ^2 remains constant as expected, with $\chi^2/\text{n. d. f.} \approx 1$. In the other cases, $\chi^2/\text{n. d. f.}$ begins to diverge rapidly after a delay dependent on model type and resolution. Beginning near 10 mg · years, we remark that the exposure at which goodness of fit begins to diverge is an order of magnitude less for the adiabatic model with 50 meV resolution than for the adiabatic model with 50 eV resolution. The exposure difference between sudden approximation divergences is even larger, separated by over two orders of magnitude, suggesting resolution has a (possibly more) significant impact on discerning between sudden and adiabatic models.

While this work requires higher exposure than the originally proposed 300 μg · years, QNR effects due to production of sterile neutrinos in data can be easily identified and distinguished from anomalous signals with enough data (assuming sudden or semi-sudden approximations). In addition, sub-eV energy resolution significantly reduces the exposure necessary for discrimination. Of course, the absolute exposure required for these procedures depends greatly on mixing angle.

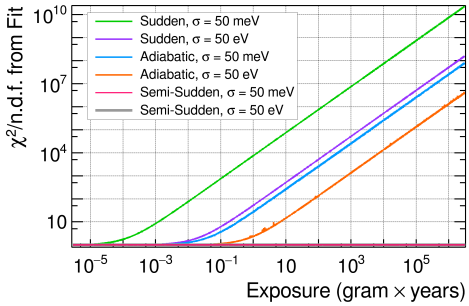


Figure 6. Average χ^2 per number of degrees of freedom for fits under various approximations and energy resolutions to semi-sudden approximation data with $\sin^2\theta = 10^{-5}$ and $m_\nu = 7$ keV as a function of exposure. χ^2 of semi-sudden derived functions (regardless of resolution) remain constant around $\chi^2/\text{n. d. f.} \approx 1$, whereas functions derived under different approximations, after a certain delay, drastically increase with exposure time. Hence, with enough exposure, data alone would indicate the type of threshold effect. Notably, this deviation is present with an order of magnitude less exposure for the 50 meV energy resolution than for the 50 eV resolution for the adiabatic approximation. In the case of sudden approximation functions, the discrepancy is over two orders of magnitude.

5. Discussion

The PTOLEMY approach to keV-scale searches for sterile neutrinos is revisited in the context of quantized nuclear-recoil effects predicted from β-decay on tritiated graphene. The sudden, semi-sudden, and adiabatic models are used to parameterize the range of theoretical uncertainty on quantized nuclear-recoil effects. This study shows that the high-resolution differential energy measurements from PTOLEMY are essential to identifying the characteristic threshold production behavior for sterile neutrinos. A clear model separation is achieved, and the quantized nuclear-recoil effects change the energy distribution near the threshold. We performed a goodness-of-fit scan for a choice of parameters describing the three models by fitting to the shape distortion and extracting the sterile neutrino signal. Direct measurement of the endpoint for fabricated tritiated-graphene samples is needed to fix the prediction for keV-scale production of sterile neutrinos in the region of the threshold. The additional handle from measuring quantized nuclear-recoil effects in the production of sterile neutrinos is a potentially powerful tool for identifying the systematic contributions that mimic a sterile-neutrino threshold.

Author Contributions: Conceptualization, C.G.T.; methodology, W.C., M.F., A.T., C.G.T. and S.Z.; software, M.F., A.T. and S.Z.; validation, M.F., A.T. and C.G.T.; formal analysis, M.F.; writing—original draft preparation, C.G.T. and M.F.; writing—review and editing, W.C., M.F., A.T. and C.G.T.; visualization, W.C.; supervision, A.T. and C.G.T. All authors have read and agreed to the published version of the manuscript.

Funding: This material is based upon work supported by the National Science Foundation Graduate Research Fellowship Program under Grant # DGE-2039656. Any opinions, findings, and conclusions or recommendations expressed in this material are those of the author(s) and do not necessarily reflect the views of the National Science Foundation.

Data Availability Statement: The original contributions presented in this study are included in the article. Further inquiries can be directed to the corresponding author.

Conflicts of Interest: The authors declare no conflicts of interest.

References

1. Tully, C.G. *Elementary Particle Physics in a Nutshell*; Princeton University Press: Princeton, NJ, USA , 2011.
2. Pontecorvo, B.M. Mesonium and antimesonium. *JETP Lett.* **1957**, *33*, 549–551.
3. Pontecorvo, B. Inverse beta processes and nonconservation of lepton charge. *Zh. Eksp. Teor. Fiz.* **1957**, *34*, 4.
4. Maki, Z.; Nakagawa, M.; Sakata, S. Remarks on the unified model of elementary particles. *Prog. Theor. Phys.* **1962**, *28*, 870–880. [CrossRef]
5. Pontecorvo, B. Neutrino experiments and the problem of conservation of leptonic charge. *Sov. Phys. JETP* **1968**, *26*, 165.
6. Gribov, V.; Pontecorvo, B. Neutrino astronomy and lepton charge. *Phys. Lett. B* **1969**, *28*, 493–496. [CrossRef]
7. de Vega, H.J.; Sanchez, N.G. Warm Dark Matter Galaxies with Central Supermassive Black Holes. *Universe* **2022**, *8*, 154. [CrossRef]
8. Shrock, R. Decay L $0 \rightarrow \nu$ l γ in Gauge Theories of Weak and Electromagnetic Interactions. *Phys. Rev. D* **1974**, *9*, 743. [CrossRef]
9. Pal, P.B.; Wolfenstein, L. Radiative Decays of Massive Neutrinos. *Phys. Rev. D* **1982**, *25*, 766. [CrossRef]
10. Foster, J.W.; Kongsore, M.; Dessert, C.; Park, Y.; Rodd, N.L.; Cranmer, K.; Safdi, B.R. Deep Search for Decaying Dark Matter with XMM-Newton Blank-Sky Observations. *Phys. Rev. Lett.* **2021**, *127*, 051101. [CrossRef]
11. Minkowski, P. $\mu \rightarrow e\gamma$ at a Rate of One Out of 10^9 Muon Decays? *Phys. Lett. B* **1977**, *67*, 421–428. [CrossRef]
12. Asaka, T.; Shaposhnikov, M. The νMSM, Dark Matter and Baryon Asymmetry of the Universe. *Phys. Lett. B* **2005**, *620*, 17–26. [CrossRef]
13. Richter, M.; Tupper, G.; Viollier, R. Neutrino Masses, Dark Matter and the Mysterious Early Quasars. *Prog. Part. Nucl. Phys.* **2010**, *64*, 449–450. [CrossRef]
14. Dodelson, S.; Widrow, L.M. Sterile Neutrinos as Dark Matter. *Phys. Rev. Lett.* **1994**, *72*, 17. [CrossRef]
15. Shi, X.; Fuller, G.M. New Dark Matter Candidate: Nonthermal Sterile Neutrinos. *Phys. Rev. Lett.* **1999**, *82*, 2832. [CrossRef]
16. Fermi, E. Versuch einer Theorie der β-Strahlen. I. *Z. Phys.* **1934**, *88*, 161–177. [CrossRef]
17. Carminati, M.; Gugiatti, M.; Siegmann, D.; Urban, K.; King, P.; Edzards, F.; Lechner, P.; Mertens, S.; Fiorini, C. The TRISTAN 166-Pixel Detector: Preliminary Results with a Planar Setup. *Nucl. Instrum. Methods Phys. Res. Sect. A Accel. Spectrom. Detect. Assoc. Equip.* **2023**, *1049*, 168046. [CrossRef]
18. Foerstner, E.; KATRIN-Collaboration. Backscattering on the KATRIN rear wall as a systematic effect for a keV-scale search for sterile neutrinos. *Verhandlungen Dtsch. Phys. Ges.* **2017**, *52*, 1.
19. Adhikari, R.; Agostini, M.; Ky, N.A.; Araki, T.; Archidiacono, M.; Bahr, M.; Baur, J.; Behrens, J.; Bezrukov, F.; Dev, P.B.; et al. A white paper on keV-scale sterile neutrino dark matter. *J. Cosmol. Astropart. Phys.* **2017**, *2017*, 025. [CrossRef]
20. Betti, M.; Biasotti, M.; Boscá, A.; Calle, F.; Canci, N.; Cavoto, G.; Chang, C.; Cocco, A.; Colijn, A.; Conrad, J.; et al. Neutrino physics with the PTOLEMY project: Active neutrino properties and the light sterile case. *J. Cosmol. Astropart. Phys.* **2019**, *2019*, 047. [CrossRef]
21. Casale, A.; Esposito, A.; Menichetti, G.; Tozzini, V. The β-decay spectrum of Tritiated graphene: Combining nuclear quantum mechanics with Density Functional Theory. *arXiv* **2025**, arXiv:2504.13259.
22. Ashtari Esfahani, A.; Böser, S.; Buzinsky, N.; Carmona-Benitez, M.; Claessens, C.; De Viveiros, L.; Doe, P.; Fertl, M.; Formaggio, J.; Gaison, J.; et al. Tritium beta spectrum measurement and neutrino mass limit from cyclotron radiation emission spectroscopy. *Phys. Rev. Lett.* **2023**, *131*, 102502. [CrossRef] [PubMed]
23. Pepe, C.; Corcione, B.; Pandolfi, F.; Garrone, H.; Monticone, E.; Rago, I.; Cavoto, G.; Apponi, A.; Ruocco, A.; Malnati, F.; et al. Detection of low-energy electrons with transition-edge sensors. *Phys. Rev. Appl.* **2024**, *22*, L041007. [CrossRef]
24. Rajteri, M.; Biasotti, M.; Faverzani, M.; Ferri, E.; Filippo, R.; Gatti, F.; Giachero, A.; Monticone, E.; Nucciotti, A.; Puiu, A. TES Microcalorimeters for PTOLEMY. *J. Low Temp. Phys.* **2019**, *199*, 138–142. [CrossRef]

Disclaimer/Publisher's Note: The statements, opinions and data contained in all publications are solely those of the individual author(s) and contributor(s) and not of MDPI and/or the editor(s). MDPI and/or the editor(s) disclaim responsibility for any injury to people or property resulting from any ideas, methods, instructions or products referred to in the content.